Full length article

Pore structure and wetting alteration combine to produce the low salinity effect on oil production

Edward Andrews [*], Ann Muggeridge, Alistair Jones, Samuel Krevor

Imperial College London, Department of Earth Science & Engineering, London, SW7 2AZ, United Kingdom

ARTICLE INFO

ABSTRACT

Low salinity water flooding is a promising enhanced oil recovery technique that has been observed, in experiments over a range of scales, to increase oil production by up to 14% in some systems. However, there is still no way of reliably predicting which systems will respond favourably to the technique. This shortcoming is partly because of a relative lack of pore scale observations of low salinity water flooding. This has led to a poor understanding of how mechanisms on the scale of micrometres lead to changes in fluid distribution on the scale of centimetres to reservoir scales. In this work, we use X-ray micro-CT scanning to image unsteady state experiments of tertiary low salinity water flooding in Berea, Castlegate, and Bunter sandstone micro-cores. We observe fluid saturations and characterise the wetting state of samples using imagery of fluid–solid fractional wetting and pore occupancy analysis. In the Berea sample, we observed an additional oil recovery of 3 percentage points during low salinity water flooding, with large volumes of oil displaced from small pores but also re-trapping of mobilised oil in large pores. In the Bunter sandstone, we observed 4 percentage point additional recovery with significant displacement of oil from small pores and no significant retrapping of oil in large pores. However, in the Castlegate sample, we observed just 1 percentage point of additional recovery and relatively small volumes of oil mobilisation. We observe a significant wettability alteration towards more water-wet conditions in the Berea and Bunter sandstones, but no significant alteration in the Castlegate sample. We hypothesise that pore structure, specifically the topology of large pores impacted recovery. We find that poor connectivity of the largest pores in each sample is strongly correlated to additional recovery. This work is the first systematic comparison of the pore scale response to low salinity flooding across multiple sandstone samples. Moreover, it gives the first pore scale insights into the role of pore geometry and topology on the mobilisation of oil during low salinity water flooding.

1. Introduction

Low salinity water flooding is an enhanced oil recovery technique which has been widely studied since the 1990s [1–5]. The technique has received great research interest because of the observed potential to improve oil recovery by up to 14% [4,6–12]. However, there are many examples of experiments where little or no incremental oil recovery during low salinity flooding is observed [13–17]. There is currently no way of reliably predicting whether low salinity water flooding will improve oil recovery in a given system [18].

Wettability alteration is thought to be the primary driver for improved recovery during low salinity waterflooding [19]. However, exactly how changes in wetting state lead to the production of oil during low salinity water flooding remains poorly understood. This lack of understanding stems from the absence of pore-resolution observations of fluid displacement over a field of view encompassing a connected

network of tens or hundreds of pores. The majority of experimental observations are either focused on determining the process by which wettability alteration occurs on a mineral surface within a single pore, or observations of saturation changes across the core-scale, where samples typically range from a few to tens of centimetres (see summary by Berg et al. [20], Buckley et al. [21], Basu and Sharma [22], Alotaibi et al. [23], Sheng [24], Jackson et al. [19]).

Over pore and pore network scales, the impact of low salinity waterflooding on oil distribution is complex and not well understood. Features such as pore structure, mineralogy and stagnant regions of high salinity brine all impact local oil distribution, leading to heterogeneous impacts across pore-network scales [25–27]. It is widely known that pore structure can have a dramatic impact on displacement mechanisms and flow regimes. Pore aspect ratios, pore radii distributions, coordination number, and pore-scale disorder have all been shown to impact flow regimes during both imbibition and drainage [28,29,29–33]. Furthermore, recent pore scale numerical simulation studies have

---

Nomenclature

Symbol

EOR	Enhanced Oil Recovery
HSB	High Salinity Brine
HSWF	High Salinity Water flooding
LSB	Low Salinity Brine
LSWF	Low Salinity Water Flooding
PV	Pore Volumes
A_{fo}	The fraction of the solid surface exposed to the pores that is coated by oil
K	Permeability
ϕ	Porosity
S_w	Water saturation
S_o	Oil saturation
σ	Interfacial tension
N_c	Capillary Number
v	Characteristic Velocity
μ	Viscosity

shown that pore size and morphology can impact oil mobilisation and retrapping during low salinity water flooding [34,35]. Despite this, no experimental study has yet investigated the impact of pore structure on the efficacy of low salinity waterflooding.

There is great potential for X-ray Micro-CT imaging technology to give valuable insights into the role of pore structure on oil production during low salinity waterflooding. In recent years, X-ray micro-CT imaging has provided important observations of pore scale behaviour during low salinity waterflooding, including direct in-situ observations of fluid redistribution, wettability alteration, osmosis events, and water film propagation [36–41]. However, pore scale imaging of low salinity waterflooding of clastic rocks has been restricted to experiments on Berea sandstone cores. Without pore scale observations of low salinity water flooding in a range of samples with varied pore structures, no clear understanding of the impact of pore structure on the efficacy of low salinity waterflooding can be developed.

In this study, we perform a systematic comparison of low salinity waterflooding of different sandstone samples with similar bulk mineralogical composition, but with different pore structures. This approach allows us to isolate the role of pore geometry and topology on the mobilisation of oil during low salinity waterflooding. We use X-ray micro-CT scanning to image unsteady state experiments of tertiary low salinity water flooding in Berea, Castlegate, and Bunter sandstone micro-cores. For each sample, we observe fluid saturations and characterise the wetting state of samples using imagery of fluid–solid fractional wetting and pore occupancy analysis. This work is the first systematic comparison of the pore scale response to low salinity flooding across multiple sandstone samples, and the first study to identify the leading role of pore structure on recovery during low salinity waterflooding.

2. Methods

2.1. Rock samples and fluid properties

In this work we make use of three datasets of low salinity water flooding applied to sandstone rocks. One experimental dataset was previously reported in Andrews et al. [39], and consists of raw X-ray micro-CT images of tertiary low salinity waterflooding experiment in a Berea sandstone core with an altered wetting state. We also present two new data sets of X-ray micro-CT images of tertiary low salinity water-flooding experiments in a Bunter sandstone and Castlegate sandstone

sample (see Fig. 1). See Table 1 for a summary of properties for each sample.

The Berea sample had a diameter of 6 mm and a length of 20 mm. The imaged porosity of the Berea sample is 0.11 (Table 1). The estimated absolute permeability value (calculated using PNFlow, as described in Section 2.4) of the Berea sample is 14 mD. This porosity value is broadly in line with other imaged porosity values of Berea sandstone, which are typically lower than absolute porosity values due to sub-resolution porosity [38,42].

Berea sandstone has been used extensively in petrophysical research [43–45]. It is predominantly made up of quartz (>70%) with smaller fractions of feldspar (<20%) and clays (predominantly kaolinite) (<10%), as well as small quantities of additional minerals such as pyrite and ankerite [45]. Surveys across Berea samples has shown a range of porosity and permeability values of $0.18 < \phi < 0.25$, and $45 < k < 1000$ mD respectively [38,46,47].

The Bunter sample had a diameter of 6 mm and a length of 15 mm. The imaged porosity of the Bunter sample is 0.15 (Table 1). The estimated absolute permeability value (calculated using PNFlow, as described in Section 2.4) of the Berea sample is 142 mD. The sample used was cut from a Triassic Sherwood Sandstone core supplied by the British Geological Survey. The mineralogy and petrophysical properties of this group varies, but is typically predominantly quartz and feldspar grains, with significant clay content (predominantly kaolinite). Surveys across samples in this group have shown a range of porosity and permeability values of $0.05 < \phi < 0.4$, and $10 < k < 600$ mD respectively [48–50].

The Castlegate sample had a diameter of 5.5 mm, a length of 15 mm. The imaged porosity of the Castlegate sample is 0.20 (Table 1). The estimated absolute permeability value (calculated using PNFlow, as described in Section 2.4) of the Castlegate sample is 495 mD. The core was cut from a block with average mineralogy of 94 wt% quartz and feldspar, and 6 wt% clay minerals, porosity in the range of $0.2 < \phi < 0.25$, and permeability in the range $550 < k < 950$ mD.

Fig. 2 shows the pore radius distribution for the three samples. The Berea sample has a distinctly different pore radius distribution compared to the Bunter and Castlegate samples. The Berea has a narrower distribution, with average values far lower than for the other two samples. The Bunter and Castlegate samples have very similar pore radius distributions.

The oil used for the experiments is a degassed Western Hemisphere crude oil with a density of 0.87 kg/m^3 and viscosity 13 mPa s at 70 °C. The oil has a total acid number of 0.01 mgKOH/g and a total base number of 2 mgKOH/g. The Saturates, Aromatics, Resins and Asphaltenes analysis data are Sat=22.00 wt%, Aro=41.00 wt%, Res=20 wt%, and Asp=17 wt%. The oil was doped with 20 wt% iododecane. This dopant concentration represents a trade-off between replicating a realistic reservoir system and the ability to reliably distinguish between phases in X-ray images We chose to add dopant to the oil, as opposed to the brines, to avoid increasing the salinity of the low salinity brine. There remains some uncertainty around the effect of iododecane on interfacial properties. A recent study by Pan and Trusler [51] has shed some light on this. The authors reported that the interfacial tension between iododecance and water was 4.5 mNm^{-1} lower than the interfacial tension between water and decane. The authors concluded that doping decane with iododecane would lead to a decrease in the water-organic phase interfacial tension. This would suggest that introducing 20 wt% iododecane into the crude oil, acts to decrease the brine–oil interfacial tension.

We used two distinct brines, the first, referred to as high salinity brine (total dissolved salt content of 73,841 mg/l) was used for the initial waterflood. The second, referred to as low salinity brine (total dissolved salt content of 1064 mg/l), was used for the second and third waterflood. Both brine recipes are shown in Table 2. The low salinity brine is simply the high salinity brine recipe diluted by a factor of 69.4.

Table 1
A summary of rock properties for the Berea, Castlegate, and Bunter samples used in this work.

	Porosity [–]	Permeability [mD]	Clay volume fraction [–]	Sample diameter [mm]	Sample length [mm]
Berea	0.11	14	0.06	6	20
Bunter	0.15	142	0.06	6	15
Castlegate	0.20	495	0.08	5.5	15
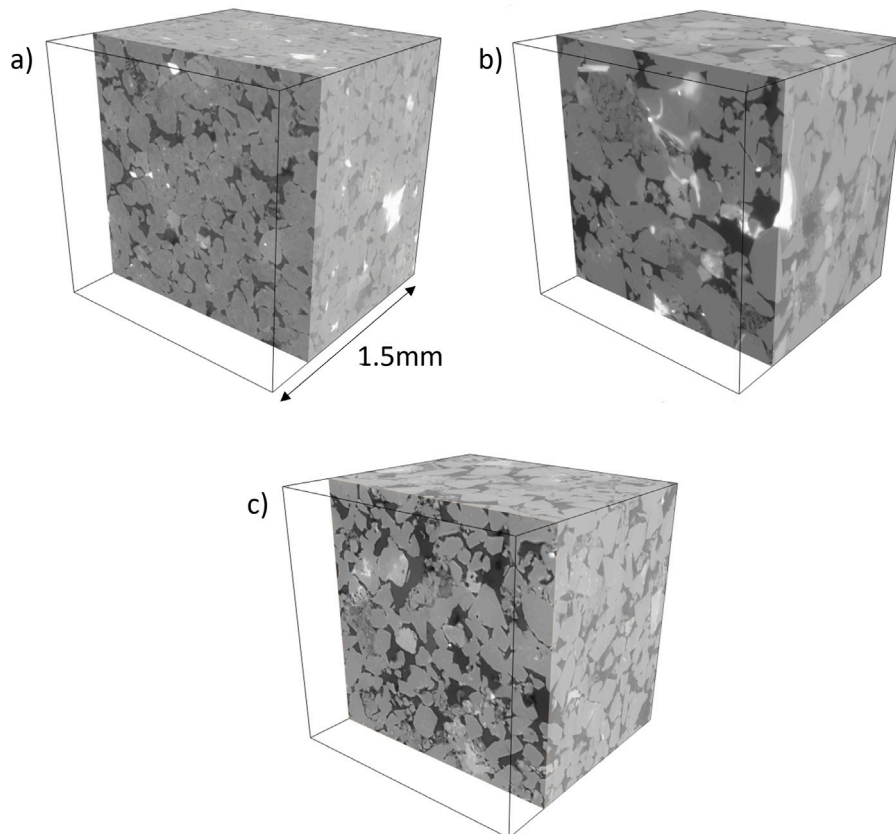
Fig. 1. X-ray micro-CT images of the three lithologies used in this work: (a) Berea sandstone; (b) Bunter sandstone; (c) Castlegate sandstone. The grey scale is linked to light attenuation, with the darker regions having the lowest density (e.g., pores) and the brightest regions comprising of the most dense materials (e.g., carbonate cement or metal oxides). All images were acquired using an FEI Heliscan micro-CT machine. The voxel sizes are 2.42 μm, 2.35 μm, and 2.31 μm.

Table 2
The brine recipes, including total dissolved salts (TDS) values, for both the high and low salinity brines used in the study. Note that the low salinity brine is simply the high salinity brine diluted by a factor of 69.4. The brine recipes used here were requested by our industry sponsor. The values are consistent with their industry approach to LSWF.

Salts	Dissolved salts [mg/l]	
	High salinity brine	Low salinity brine
$CaCl_2.2H_2O$	13205	190
$MgCl_2.6H_2O$	2008	29
KCl	744	11
NaCl	57884	834
TDS	73,841	1,064

2.2. Flow experiments

Each sample was placed into a carbon fibre Hassler type flow cell, which was used to keep the rocks under pressure with a confining fluid (water). The samples were placed in a Viton sleeve, and connected to a hydraulic circuit with two steel end pieces. The cell was then placed into an X-ray μ-CT scanner so that images could be taken at each stage of the experiment.

After loading the samples into the core holder, we began flow experiments using the below workflow (see Fig. 3). For all flow steps,

a confining pressure of 50 bar was maintained within the core holder. This compresses the Viton sleeve around the cores, therefore, preventing fluid bypassing the samples. An inlet pressure of 30 bar was maintained at all times. The experiments were carried out at ambient temperatures, approximately 25 °C.

High salinity brine was first pumped through each sample at 0.2 ml/min for 30 min to saturate the sample fully. Undoped crude oil was then pumped through the samples at 0.015 ml/min for 10 pore volumes (PV). This flow rate was sufficient to displace the vast majority of brine from each sample. We observe that following the oil flood, S_w was <0.05 for all three samples. The wetting state of the cores was then altered: the samples were submerged in a sealed beaker of undoped crude oil for four weeks at 80 °C. Next, high salinity brine was pumped through the samples for a total of 12 PV. Four PV of low salinity brine was then injected, followed by a final 16 PV of low salinity brine injection, making a total of 20 PV of low salinity flooding. For the Bunter and Castlegate samples, a flow rate of 0.015 ml/min was maintained for the doped oil injection and subsequent waterfloods at an injection pressure of 30 bar giving an approximate capillary number for the waterfloods of $N_c = v\mu/\sigma = 3 \times 10^{-7}$ and 3.6×10^{-7} respectively. For the Berea sample, we could not achieve a flow rate of 0.015 ml/min at an injection pressure of 30 bar for the doped oil injection and subsequent waterfloods. Instead, we maintained a constant pressure
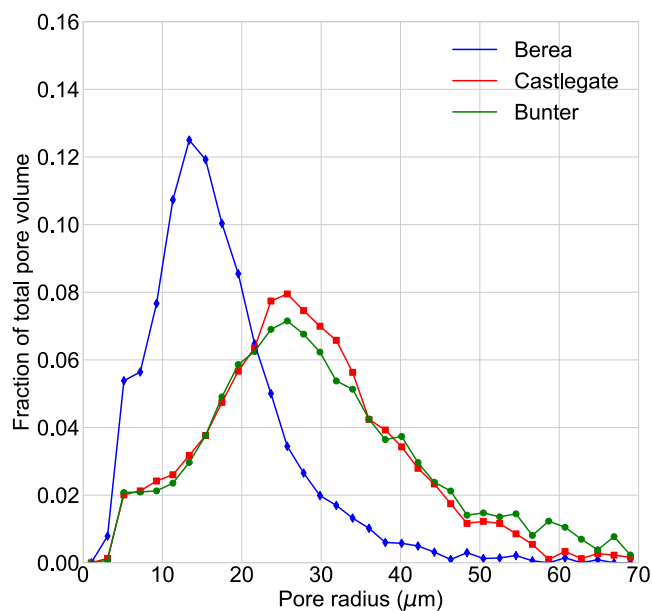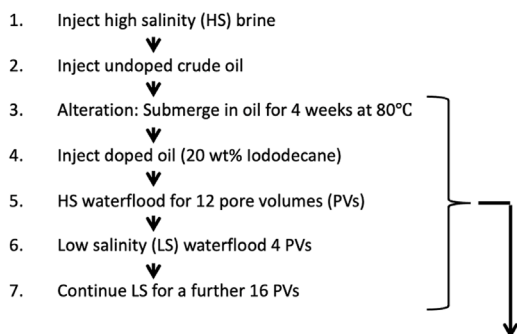
Fig. 2. Plot of pore radius distributions as a fraction of total pore volume for each sample. The Berea sandstone sample (blue) has a far narrower pore size distribution than the Bunter (green) and Castlegate (red) samples which have a very similar profile. (For interpretation of the references to colour in this figure legend, the reader is referred to the web version of this article.)

Fig. 3. An overview of the experimental workflow for all samples. We chose to carry out tertiary low salinity flooding experiments, as opposed to secondary low salinity flooding, so that the incremental additional recovery from low salinity flooding could be more confidently determined. A more detailed description of the workflow can be found in the text.

differential of 25 bar from the inlet to the outlet of the core for these flow steps. This resulted in an average flow rate of 0.001 ml/min, giving an approximate capillary number for the waterfloods of $N_c = 2 \times 10^{-8}$. Evidently, the wettability alteration process in the Berea sandstone led to a reduction in permeability, possibly because of the precipitation of asphaltenes.

The values of 4 PV and 20 PV of low salinity flooding for each sample were carefully chosen so that both the initial and final response to low salinity flooding could be observed. Khishvand et al. [37] observed an initial shift in wetting state and pore occupancy between 0.5 and 5 PV of low salinity flooding in a Berea sample. We chose a value of 4 PV to be broadly consistent with Khishvand et al. [37], and to maximise the probability of observing oil banking. A further 16 PV of low salinity flooding was carried out to displace any banked oil, and maximise oil recovery.

2.3. Image acquisition and analysis

The samples were imaged with an FEI Heliscan micro-CT instrument obtaining a voxel size of 2.4 μm for a region of interest larger than the sample cross section and a vertical length of 9 mm for the Berea, 5.5 mm for the Castlegate, and 7 mm for the Bunter. The tube current was set to 70 mA and the X-ray source voltage to 95 k. The raw images were then reconstructed using iterative back projection algorithms provided by the scanner manufacturer.

For each sample a region of interest was extracted from all scans. In the Berea, a region of interest of 1500 × 1500 × 3500 voxels (3.6 ×3.6× 8.4 mms) was extracted; for the Castlegate, the region of interest was 1425 × 1425 × 2375 voxels (3.3×3.3× 5.5 mms); for the Bunter, the region of interest was 1500 × 1500 × 3000 voxels (3.5 ×3.5× 7.0 mms). Next, the signal to noise ratio of all images was increased using a non-local means filter [52].

The undoped scans (Fig. 4a, b, and c) for each sample were then segmented into 3 phases (Fig. 4d, e, and f) – the pore space, and two mineral groups, namely, clays and all minerals, excluding clays – using a watershed segmentation [53]. The segmented pore space was then used to mask all subsequent scans for each sample. After each image was masked, just the fluid phases remained and thresholding was used to segment the brine and oil. In each case, the threshold value was determined by the histogram of grey values. The segmented fluid phases were then combined with the clay segmentation. Lastly, an erosion/dilation tool was used to remove any erroneous layers with a thickness of one voxel from the mineral surfaces.

2.4. Estimating saturation, surface area coverage, and pore occupancy

The fluid saturation across the region of interest was estimated using the segmented images where the water saturation, S_w, the fractional volume of the water volume in the pore space was averaged across each of the horizontal slices in each dataset. A saturation profile was produced for each sample by stacking the saturation values along the length of the region of interest.

We then assess the fraction of mineral surfaces coated by a fluid phase, A_{fi}. This is defined, using segmented images of each sample at each flow step, as the amount of the solid surface exposed to the pores that is covered a fluid phase, A_i, divided by the total amount of solid surface exposed to the pores, A_T. For oil, $A_{fo} = A_o/A_T$. Whilst there are some sources of uncertainty in this approach, in particular the ability to resolve thin water films, this method has been demonstrated in [54,55] to provide a robust measure of wetting state over pore and pore-network scales. The more wetting a fluid, the greater fraction of the rock surfaces will be coated by that fluid at a given saturation. Following the workflow developed by Garfi et al. [54], the region of interest in each sample was subdivided into equal sub volumes. For the Berea, this was 63 equal subvolumes of 500 voxels per side; for the Bunter, there were 54 equal subvolumes of 500 voxels per side For each subvolume; for the Castlegate, there were 45 equal subvolumes of 475 voxels per side. For each subvolume, in each sample, brine–rock interfacial area, oil–rock interfacial area, and fluid saturations were computed. The oil–rock interfacial area as a fraction of total fluid–rock interfacial area was then calculated as a function of saturation for each of the subvolumes in each sample after all flow steps.

Next, we evaluated the sizes of the pores occupied by the fluid phases using a pore network abstraction of the pore space, using a workflow first introduced by Bultreys et al. [56]. We used a maximal ball network extraction code to extract a network of nodes, representing pores and links, representing throats, from the segmented undoped scan of each sample. Inscribed spheres were fitted to each pore, where the diameter of said spheres represents the pore diameters [57,58].

To analyse the absolute permeability of each sample, and the network of largest pores extracted from each sample, we used PNflow, an
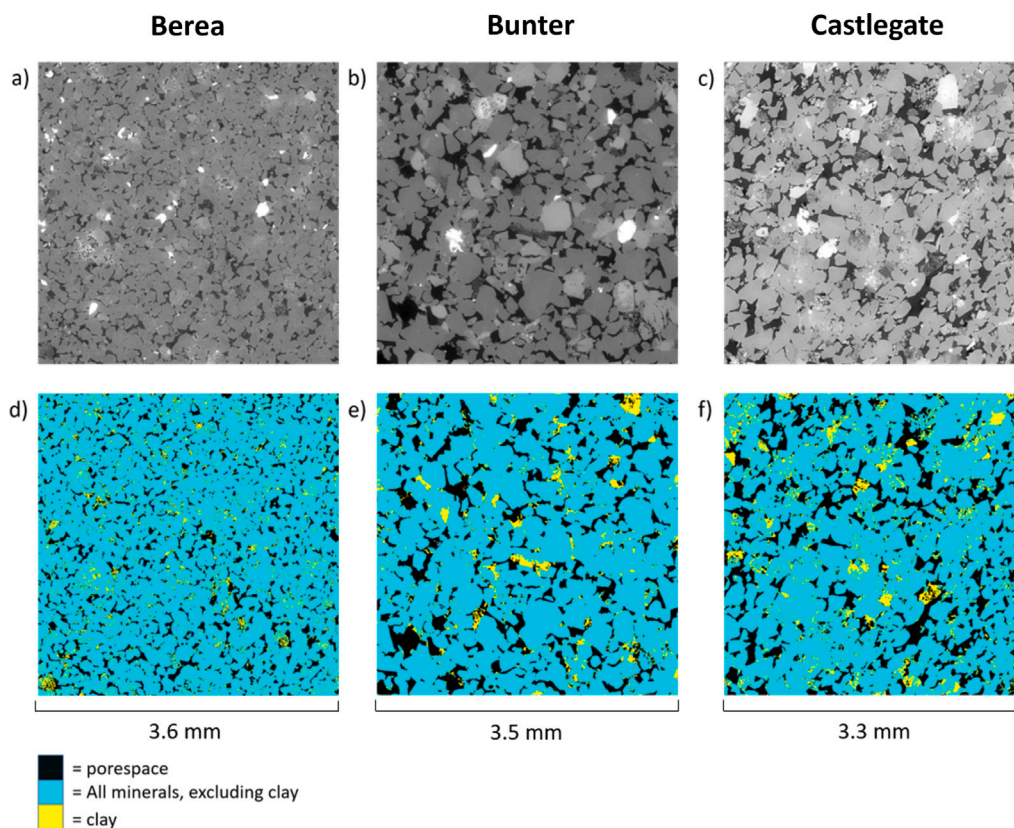
Berea	Bunter	Castlegate

Fig. 4. A slice of the X-ray micro-CT image of the (a) Berea sample (b) Castlegate sample and (c) Bunter sample, before the injection of doped oil. In each case the darkest colour represents the pore space. The corresponding slices for the segmented images of the (d) Berea sample, (e) Castlegate sample, and (e) Bunter sample are also shown, where black represents the pore space, yellow represents clay minerals, and blue represents all minerals, excluding clay. (For interpretation of the references to colour in this figure legend, the reader is referred to the web version of this article.)

open source pore network modelling tool which relies on an assumption of quasi-static capillary dominated flow. The algorithm uses the approach of Valvatne and Blunt [59], as described in Raeini et al. [60], and further validated by Raeini et al. [61] and Bultreys et al. [56]. We used PNflow to simulate single phase flow experiments to estimate absolute permeability values for each sample.

To analyse the impact of the topology of the largest pores on recovery during low salinity flooding in each sample. we first isolated the largest pores which make up 60% of total pore volume in each sample. This equates to all pores of radius > 14 μm in the Berea, 25 μm in the Castlegate, and 24 μm in the Bunter. We chose this cut-off as the minimum pore radius in this group approximately equates to the largest pores in which the oil saturation decreases during low salinity flooding in each sample. Additionally, the average S_w of pores within this group is >0.5 for all samples after each waterflood. Therefore, the connectivity of these pores is likely to impact the connectivity of the brine in each sample. We then repeated the pore network extraction and single phase flow simulations, described above, for these larger pores only, to obtain the estimates for fluid occupancy and absolute permeability in for the network of largest pores in each sample.

3. Results and discussion

3.1. Saturation distribution

Table 3 presents $\bar{S}_w$ values for each of the three samples after each waterflood step. After 20PV of low salinity flooding, there is a 3, 4, and 1 percentage point additional recovery in the Berea, Bunter and Castlegate samples respectively. Fig. 5 shows the saturation profiles for each of the three samples after each waterflood step. In all samples, there is significant variation in S_w along the length of the samples

for all waterfloods. In the Berea and Bunter samples, a significant decrease in S_w is observed in some sections towards the top of the imaged region, away from the inlet, after 4 PV of low salinity water flooding. This probably represents an accumulation of oil displaced from upstream of the imaged region during the 4 PV of low salinity flooding. This effect is most significant in the Berea sample, where there is a 1 percentage point increase in oil saturation in the region of interest after 4 PV of low salinity flooding in the Berea sample. In both samples, after 20 PV of low salinity flooding, the majority of this accumulated oil is produced from the region of interest. As a result, there is an additional oil production of 3 and 4 percentage points in the Berea and Bunter samples after 20 PV of low salinity waterflooding. These values are consistent with multiple studies carried out on sandstones at similar conditions: Lebedeva and Fogden [62] observed an additional recovery of 7 percentage points during low salinity flooding of a kaolinite coated sandpack; Chen et al. [41] reported a recovery of 5 percentage points after tertiary low salinity flooding in Berea Sandstone; and Shabaninejad et al. [38] observed a recovery of 3 percentage points in a tertiary low salinity waterflood in a Berea sandstone sample.

In the Castlegate sample, there is little change in average S_w after 4 and 20 PV of low salinity water flooding, with 1 percentage point additional recovery after 20 PV of low salinity waterflooding. Additionally the local changes in S_w values after 4 and 20 PV of low salinity flooding are significantly smaller than the changes observed in both the Berea and Bunter samples.

In the Berea and Bunter samples, a significant decrease in S_w is observed in some sections towards the top of the imaged region, away from the inlet, after 4 PV of low salinity flooding. This most likely represents an accumulation of oil displaced from upstream of the imaged region during the 4 PV of low salinity flooding. This effect is most significant in the Berea sample, where there is a 1 percentage

Table 3

Average water saturation, $\bar{S}_w$, in the region of interest, for all samples, after 12 PV of high salinity flooding (HSWF), 4 PV of low salinity water flooding (LSWF 4 PV), and 20 PV of low salinity water flooding (LSWF 20 PV). Additionally, ΔS_w relative to HSWF 12 PV is presented for all samples after LSWF 4 PV and LSWF 20 PV. In all cases, there was a very high initial oil saturation with $\bar{S}_w < 0.05$ prior to waterflooding.

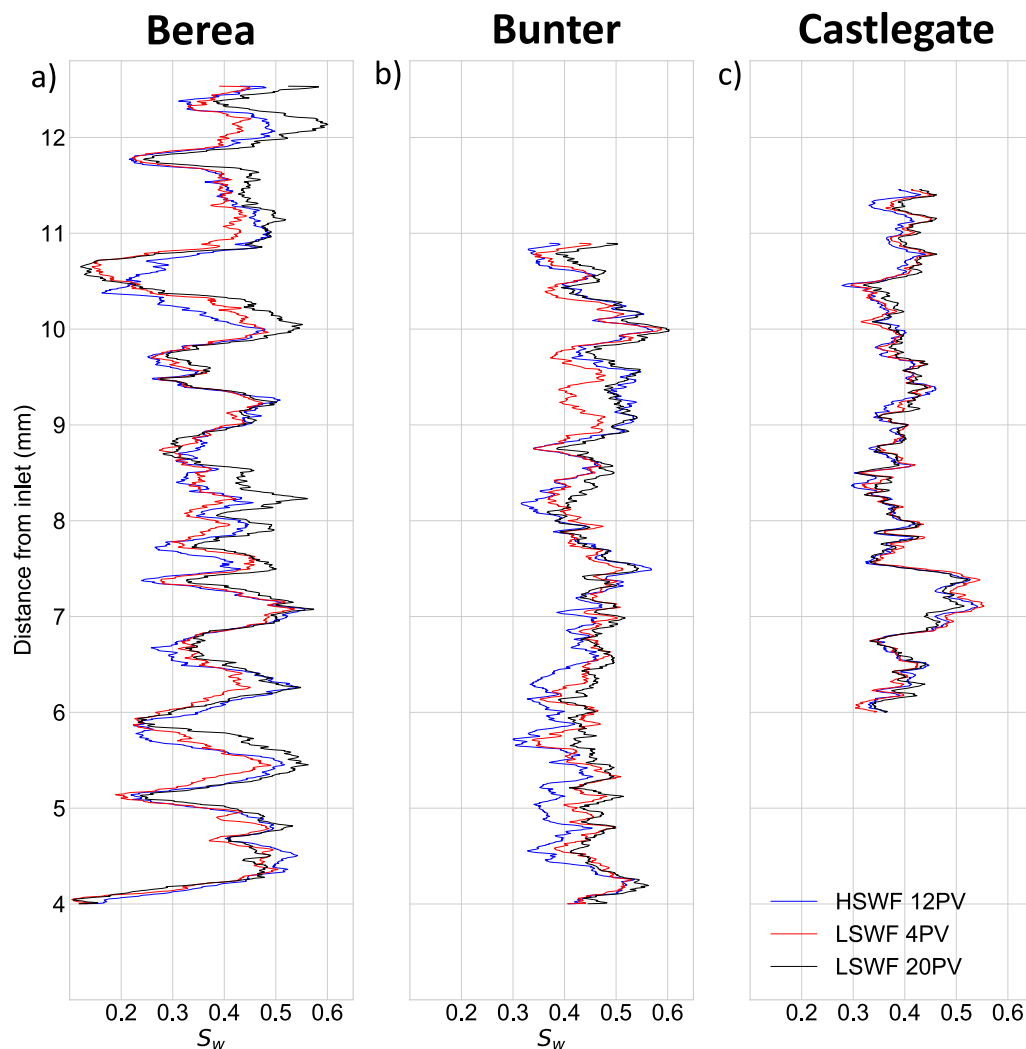|	Berea		Bunter		Castlegate	
	$\bar{S}_w$	ΔS_w relative to HSWF 12 PV	$\bar{S}_w$	ΔS_w relative to HSWF 12 PV	$\bar{S}_w$	ΔS_w relative to HSWF 12 PV
HSWF 12 PV	0.382		0.429		0.389	
LSWF 4 PV	0.368	−0.014	0.439	0.01	0.397	0.008
LSWF 20 PV	0.413	0.031	0.467	0.038	0.400	0.011

Fig. 5. Profile of water saturation, S_w, averaged perpendicular to the flooding direction across the region of interests of (a) Berea sandstone (b) Bunter sandstone (c) Castlegate sandstone after 12 PV of high salinity water flooding (HSWF 12PV), 4 PV of low salinity water flooding (LSWF 4PV), and 20 PV of low salinity water flooding (LSWF 20PV).

point increase in oil saturation in the region of interest after four pore volumes of low salinity flooding in the Berea sample. In both samples, after twenty pore volumes of low salinity flooding, the majority of this accumulated oil is produced from the imaged region.

3.1.1. Surface area fractional coverage

In Andrews et al. [39] we applied a workflow developed by Garfi et al. [54] to use bulk fluid surface area coverage measurements to show a wettability alteration. The Berea sandstone exhibited an alteration towards more water-wetting conditions, after 20 PV of low salinity water flooding. Here, we also apply this analysis to the Bunter and Castlegate samples (Fig. 6).

After high salinity water flooding, the fraction of mineral surface area coated by oil at a given saturation, $A_{fo}(S_o)$, lies above the 1:1

line for all subvolumes in all samples. This is indicative of oil-wetting behaviour, where $A_{fo} > S_o$. The oil-wetting behaviour in each sample is likely a result of the high asphaltene content (17 wt%) of the crude oil used in the experiments. It is widely understood that exposure to crude oil with a higher asphaltene content leads to more oil-wetting behaviour [63,64]. After high salinity water flooding, $A_{fo}(S_o)$ values are lower in the Berea sample than for the Bunter and Castlegate samples. For the Berea sample, $A_{fo}(S_o)$ values lie close to the 1:1 line after high salinity flooding. In contrast, $A_{fo}(S_o)$ values are significantly higher in both the Bunter and Castlegate sandstones. This suggests that the Berea sample is less oil wetting after aging than the other two samples. In all samples, we observe oil wetting behaviour after high salinity water flooding, where $A_{fo} > S_o$ for all subvolumes.
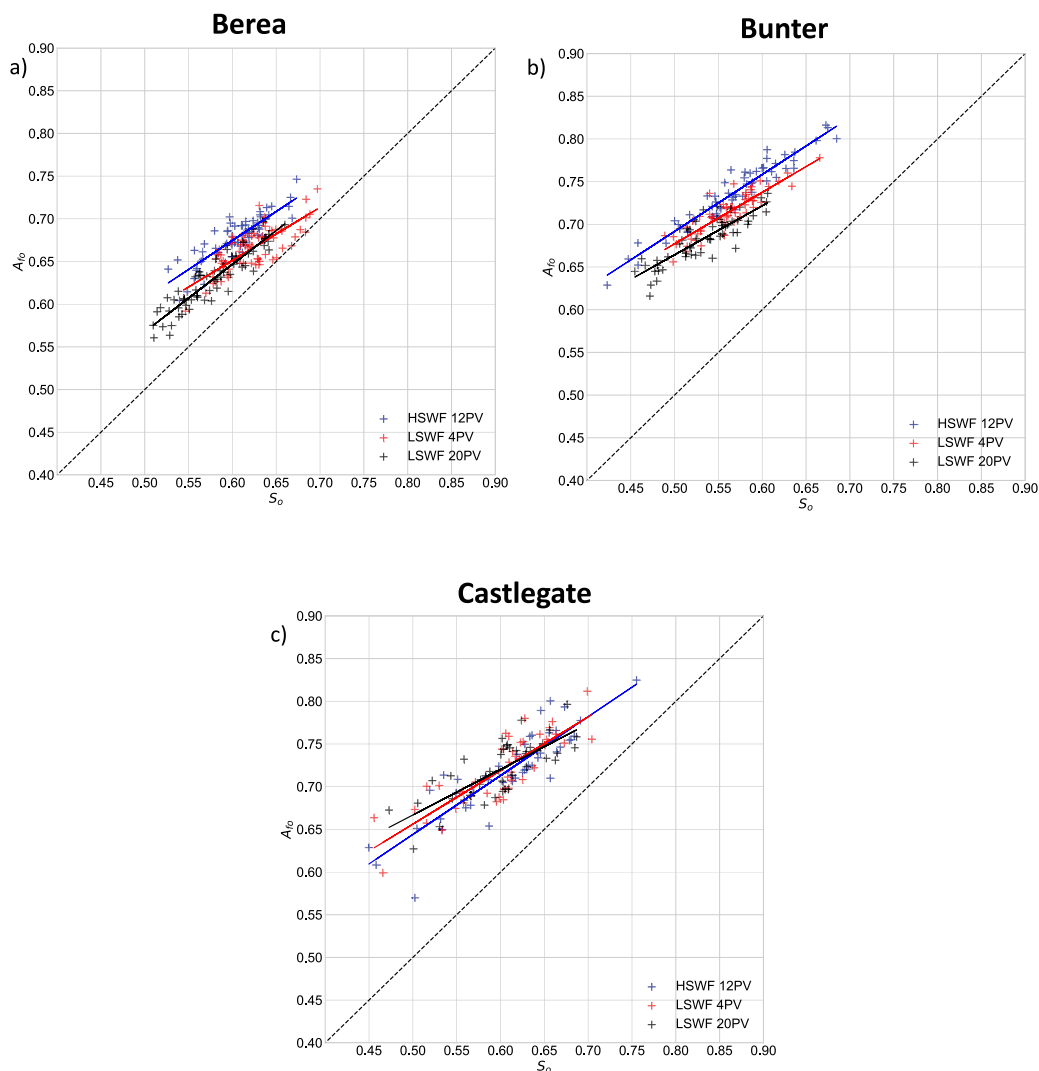
Fig. 6. Oil-coated area fractions, imaged after high salinity water flooding (HSWF), 4 PV of low salinity flooding (LSWF 4PV), and 20 PV of low salinity flooding (LSWF 20PV), for (a) Berea (b) Bunter and (c) Castlegate.

After high salinity water flooding, the fraction of mineral surface area coated by oil at a given saturation, $A_{fo}(S_o)$, is lower in the Berea sample than for the Bunter and Castlegate samples. For the Berea sample, $A_{fo}(S_o)$ values lie close to the 1:1 line after high salinity flooding. In contrast, $A_{fo}(S_o)$ values are significantly higher in both the Bunter and Castlegate sandstones. This suggests that the Berea sample is less oil wetting after aging than the other two samples. In all samples, we observe oil wetting behaviour after high salinity water flooding, where $A_{fo} > S_o$ for all subvolumes. This may have been aided by the high asphaltene content (17 wt%) of the crude oil. It is widely understood that a higher asphaltene content leads to more oil-wetting behaviour after ageing [63,64].

In the Berea sample, after 4 PV of tertiary low salinity flooding, there is a shift to lower $A_{fo}(S_o)$ values, so that for a given S_o there is a lower fraction of oil coating the mineral surfaces. This indicates a shift to more water-wet conditions. After 20 PV of tertiary low salinity flooding, there is no further shift in $A_{fo}(S_o)$ values beyond what was observed after 4 PV. However, there is a significant decrease in oil saturation, that is, in the Berea sandstone, low salinity flooding was characterised by a rapid wetting state shift, followed by oil production over longer timescales.

The Bunter sandstone responds similarly as the Berea sandstone. There is a significant shift to lower $A_{fo}(S_o)$ values after 4 PV of tertiary low salinity flooding. Between 4 and 20 PV of tertiary low

salinity flooding there is no further shift in $A_{fo}(S_o)$, however, there is a significant decrease in the oil saturation. Similarly to the Berea sandstone, in the Bunter sandstone, low salinity flooding causes a rapid wetting state shift, followed by oil production over longer timescales.

In the Castlegate sample, there is no significant shift in $A_{fo}(S_o)$ values after either 4 or 20 PV of low salinity water flooding. There is also very little oil production throughout the flooding. This suggests no systematic wettability alteration within the sample.

Observations of wettability alteration in the Berea and Bunter sandstone samples are broadly consistent with a wealth of observations of wettability alteration during low salinity waterflooding across a range of scales, from sub pore scale to field scale [11,20,65–72]. More specifically, these findings agree with pore scale observations of wetting alteration during low salinity water flooding of Berea sandstone using manual contact angle measurements [37], and observations of water-film propagation during low salinity flooding of Berea sandstone [41].

In Andrews et al. [39] we carried out an unsteady state tertiary low salinity flooding experiment using a water wet Berea sandstone sample. The experimental and image analysis workflows used were identical to those used for the Berea, Bunter and Castlegate samples in this study. In the water-wet Berea experiment, we observed very little fluid redistribution during 4 or 20 PV of low salinity waterflooding. We observed very small changes in average saturation, area fraction
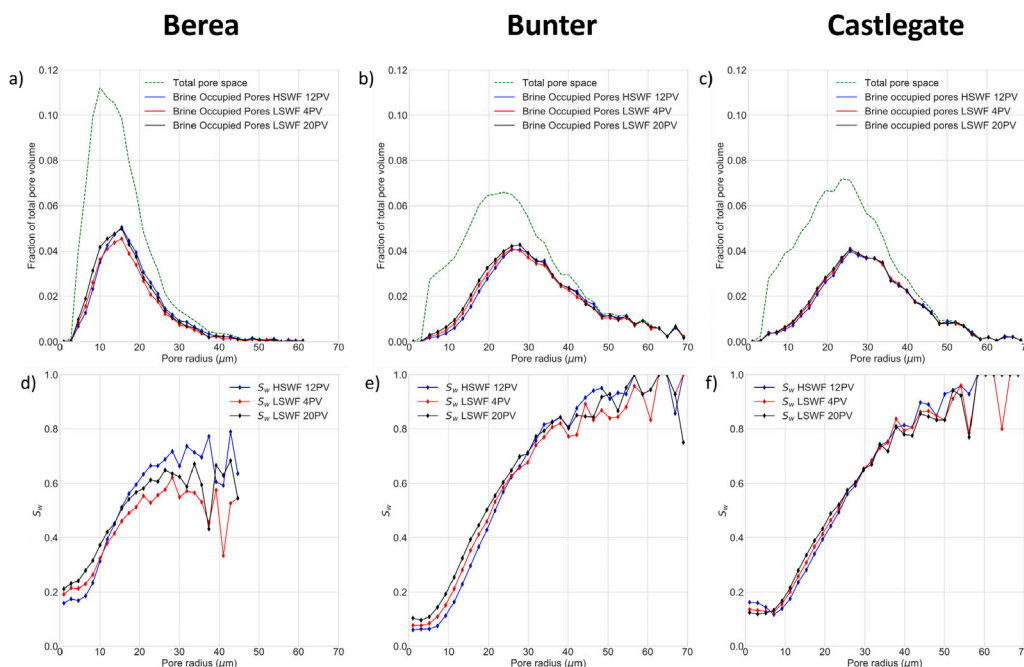
Fig. 7. The size distribution for all brine saturated pores (bodies and throats) in (a) Berea (b) Bunter (c) Castlegate, and the total brine saturation (S_w) in pore radius bins, for (d) Berea (e) Bunter (e) Castlegate, imaged after 12 PV of high salinity water flooding (HSWF 12PV), 4 PV of low salinity water flooding (LSWF 4PV), and 20 PV of low salinity flooding (LSWF 20PV).

and pore occupancy measurements between the three waterfloods, indicating that the image analysis workflow is robust and repeatable. S_w values of 0.260, 0.256 and 0.254 were recorded after high salinity water flooding, 4 PV of low salinity water flooding and 20 PV of low salinity waterflooding, respectively. This gives a mean value of 0.257, and a standard error of 0.00125. The average A_{fo} value for all subvolumes was calculated as 0.641, 0.646 and 0.646 after high salinity water flooding, 4 PV of low salinity water flooding and 20 PV of low salinity waterflooding, respectively. This gives a mean value of 0.644 and a standard error 0f 0.00118. These standard errors are an order of magnitude lower than the shifts in S_w and A_{fo} observed during low salinity flooding in the Berea and Bunter samples in this study. This highlights the robust nature of the image analysis workflows used in this work.

3.1.2. Global pore occupancy

Changes in wetting state impact the distribution of fluids throughout a sample. Here, we investigate the spatial distribution of brine saturated pores and throats after each flow step in each sample, to infer changes in wetting state, and analyse the effect of low salinity water flooding on fluid occupancy. Fig. 7 shows the contribution of different pore and throat size ranges to the total volume of brine within the region of interest of imaged in each sample.

After high salinity waterflooding, the Bunter and Castlegate samples have very similar pore occupancy profiles, with <20% of the smallest pores brine saturated, and >80% of the largest pores brine saturated (Figs. 7e and 7f). This is indicative of an oil-wet system, where it is preferable for brine to occupy the largest pores, and oil the smallest [30]. Pore occupancy after high salinity water flooding differs in the Berea sample as although <20% of the smallest pores are brine saturated, <80% of the largest pores are also brine saturated (Fig. 7d). It, therefore, appears that the Berea sample is not as strongly oil-wet as the other two samples. This agrees with the surface area fraction analysis (Fig. 6), which showed that the Berea sample is less oil-wetting compared to the Bunter and Castlegate samples, signified by lower average A_{fo} values for a given S_o in the Berea sandstone.

In both the Berea and Bunter samples, there is a significant shift in pore occupancy in the smallest pores after low salinity waterflooding.

In the Bunter sample, there is a significant increase in brine saturation in pores with radius <30 μm after 4 PV of low salinity waterflooding, and then again after 20 PV of low salinity waterflooding. We observe the same effect in the Berea, but with pores of radius <15 μm.

In the Castlegate sample, we observe a far smaller, yet systematic, increase in brine saturation in pores with radius <25 μm after both 4 and 20 PV of low salinity waterflooding. The smaller changes in pore occupancy observed in the Castlegate sample after low salinity waterflooding is expected based on the lack of pervasive and systematic wettability alteration observed using surface area fractional coverage analysis (see Fig. 6). We cannot rule out smaller local shifts in wetting state, which may explain the small shift in pore occupancy observed in the Castlegate sample.

There is little significant change in the pore occupancy of the larger pores in the Bunter and Castlegate samples (radius > 30 μm and >25 μm respectively) after low salinity flooding. However, in the Berea sample there is a significant decrease in the brine saturation in pores of radius >15 μm after low salinity water flooding. This is particularly prominent after 4 PV of low salinity waterflooding, where, on average, S_w decreases by over 10 percentage points in pores of radius >20 μm radius. Some of this redistributed oil is produced after 20 PV of low salinity waterflooding, however, S_w remains significantly lower after 20 PV of low salinity waterflooding than after high salinity waterflooding.

The systematic and consistent nature of pore occupancy changes in the smallest pores of each sample are striking. Although the effect is smaller in the Castlegate sample, in each case, there is an increase in water saturation in the smallest pores after both 4 and 20 PV of low salinity waterflooding. This change is consistent with a wettability alteration towards more water wet conditions and in broad agreement with literature. Pore occupancy results agree with experimental studies across both sandstones and carbonates [36,37,73] and modelling [27] results which show an oil reduction range in the small and medium pores during low salinity waterflooding. In all cases, this effect is thought to directly result from a wettability alteration to more water-wetting conditions during low salinity flooding. The alteration allows water to more-easily enter smaller pores and throats because of the support of capillary forces [27,36].
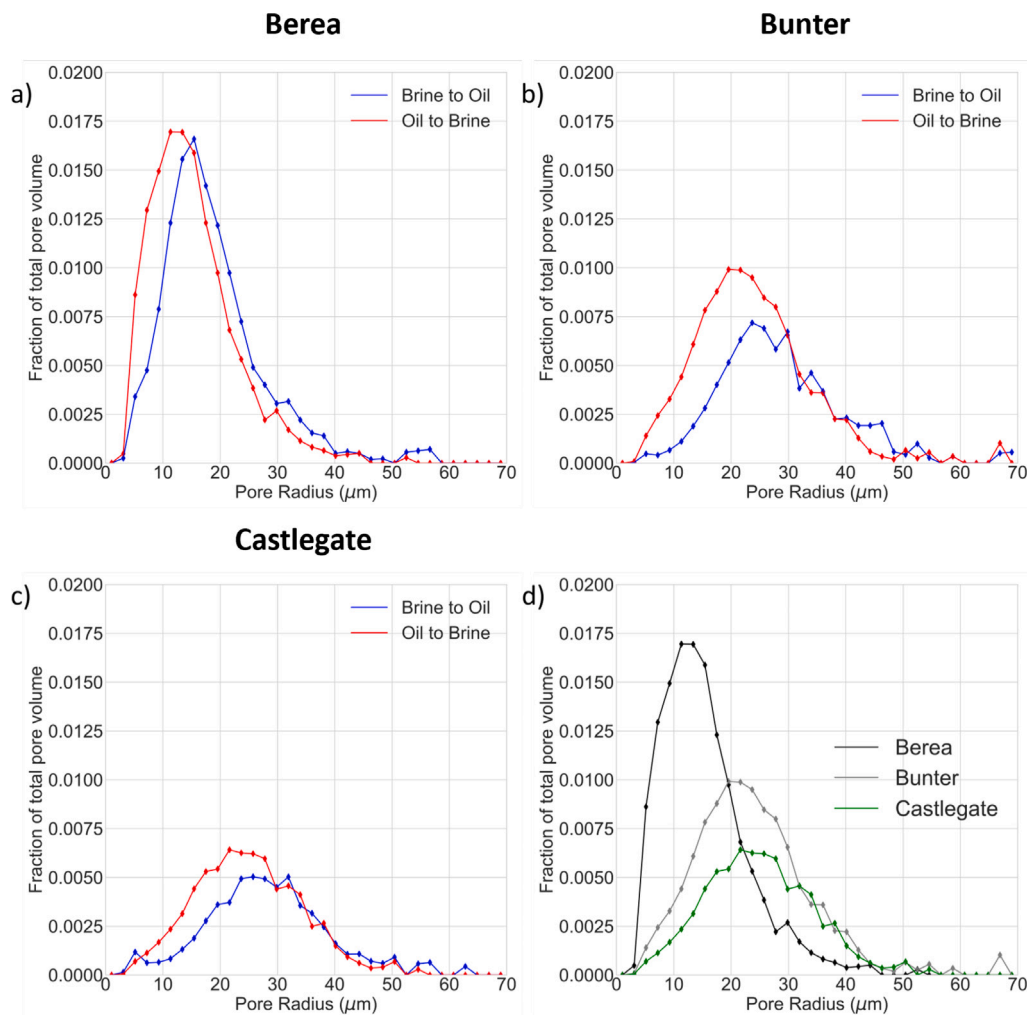
Berea

Bunter

Castlegate

Fig. 8. The size distribution for all pores (bodies and throats) where saturation changed from oil to brine (red) or brine to oil (blue) between HSWF and LSWF 20PV, for (a) the Berea sample (b) the Bunter sample (c) the Castlegate sample (d) oil to brine events in all samples. In all cases, there are more oil to brine events than brine to oil events in the medium and small pores. This effect is most significant in the Bunter sample. In the Berea sample, there are more brine to oil events than oil to brine events in the larger pores. This effect is not observed on the same scale in the Bunter and Castlegate samples. There are fewest oil to brine events in the Castlegate sample, indicative of less oil mobilisation during low salinity water flooding. (For interpretation of the references to colour in this figure legend, the reader is referred to the web version of this article.)

3.1.3. Fluid mobilisation and redistribution

To further investigate changes in pore occupancy, we isolated pores where pore occupancy changed between the high salinity waterflood and 20 PV of low salinity water flooding. In other words, we isolated pores where either brine displaced oil or oil displaced brine during 20 PV of low salinity water flooding. Fig. 8 shows the size distribution of pores in which pore occupancy changed between the flow steps for each sample.

There is a significantly higher volume of oil to brine events in the small pores (<15 μm in the Berea, <30 μm in the Bunter) in the Berea sample than in the Bunter sample, which in turn has a significantly higher volume of oil to brine events than the Castlegate sample. This is most clear in Fig. 8d which compares oil to brine events for each sample. Pores where an oil to brine event occurred account for 14% of Berea pore volume, 11% of Bunter pore volume, and 7% of Castlegate pore volume.

Despite fewer oil to brine events in the Bunter sandstone compared to the Berea, we have shown that the Bunter sandstone has the highest additional recovery after low salinity waterflooding (Fig. 5). This is appears to be because in the Bunter sample a smaller percentage of the mobilised oil is re-trapped in the larger pores. In the Berea sample, for pores >15 μm radius, brine to oil events outweigh the oil to brine events, in other words there is a net increase in S_o in the largest pores

in the Berea sample. This represents a redistribution of oil from smaller to larger pores in the Berea sample. This effect is not observed in either the Bunter or Castlegate samples.

It is important to note that, while pore occupancy analysis offers insight into changes in the distribution of fluids throughout each sample, the method may systematically underestimate saturation changes. This is because pore occupancy analysis does not take into account saturation changes in pore corners and oil layers since pore occupancy is decided based on the phase in the centre of a given pore. To more accurately assess the volume of mobilised and retrapped oil, we calculate the volume of oil that is mobilised after low salinity flooding, defined as the total fraction of oil displaced by brine after 20 PV of low salinity flooding. We compare this to bulk changes in saturation to calculate the fraction of the mobilised oil that is produced. Table 4 shows volumes of mobilised and produced oil for each sample after 20 PV of low salinity waterflooding. In the Berea and Bunter sandstones, we observe that similar fractions of the oil in place after high salinity flooding is mobilised during low salinity flooding, with values of 22% and 20%, respectively. In contrast, in the Castlegate sample, 11% of the oil in place after high salinity flooding is mobilised during low salinity waterflooding.

The difference in overall recovery between the Berea and Bunter samples is due to a significant difference in the fraction of mobilised

Table 4

The fraction of the oil in place after high salinity water flooding that is mobilised during 20 PV of low salinity water flooding in the Berea, Bunter and Castlegate samples, and the fraction of this mobilised oil that is produced.

	Fraction of OOIP mobilised [–]	Fraction of mobilised oil produced [–]	Additional recovery [percentage points]
Berea	0.22	0.20	3
Bunter	0.20	0.32	4
Castlegate	0.11	0.13	1

oil that is produced. In the Berea, 20% of mobilised oil is produced, in the Bunter, 32% of the mobilised oil is produced. This results in a slightly higher recovery in the Bunter sandstone despite a slightly lower proportion of the oil in place after high salinity flooding being mobilised during low salinity waterflooding. The pore occupancy plots give insight into why this is the case (Figs. 7 and 8). As described above, some of the oil displaced from the smallest pores in the Berea is re-trapped in the largest pores. This leads to a lower fraction of mobilised oil produced and hence a lower additional oil recovery after low salinity waterflooding. We do not observe this effect in the Bunter sample.

3.2. Linking observations to pore geometry and topology

There were different responses to low salinity flooding in each sample, despite similar mineralogy. It is possible that subtle differences in mineralogy and surface characteristics between the three samples impacted the response to low salinity flooding in each case. However, the most significant difference between the three samples is pore structure. We hypothesise that pore structure was the most significant controlling factor in the varied responses to low salinity flooding. Pore structure has been shown to impact displacement mechanisms and flow regimes in various systems with aspect ratios, connectivity, pore radius distributions, coordination number, and pore-scale disorder controlling behaviour during both imbibition and drainage [28–33]. However, the role of pore structure in facilitating additional recovery during low salinity flooding has yet to be investigated thoroughly. In this section, we present evidence to show the topology of the largest pores is important in determining the volume of oil mobilisation and production during tertiary low salinity water flooding.

A notable difference in the pore structure of each sample is the connectivity of the largest pores. Fig. 9 shows a volume rendering of the largest pores accounting for 60% of total pore volume in each sample. The largest pores connect across the region of interest in the Castlegate sample, but not the Bunter and Berea samples. In the Berea sample, the large pores are poorly connected, with the largest connected cluster of large pores accounting for only 20% of the total volume of large pores in the Berea sample. In the Castlegate sample, the vast majority of the largest pores are connected across the region of interest, this connected pathway makes up 89% of the total volume of the largest pores in the castlegate sample. In the Bunter sample, there are two distinct behaviours, in the upstream section, the large pores are poorly connected, similar to the Berea sample, and in the downstream section there is a connected pathway of large pores, similar to the Castlegate sample. The largest connected cluster of large pores in the Bunter sample makes up 57% of the total volume of large pores, and is located in the upper section of the sample. In both the Berea and Bunter samples the network of the largest pores do not connect across the region of interest, and so the permeability calculated across both networks is zero. In contrast, we calculate an absolute permeability value of 27 mD across the network of the largest pores in the Castlegate samples (Table 5) using PNflow as described in Section 2.4.

The connectivity of the largest pores in each sample controls the brine distribution and, therefore, the mobilisation or bypassing of oil during low salinity waterflooding. The largest brine blob in the Castlegate region of interest after high salinity waterflooding accounts for 60% of total brine volume, and connects in a continuous pathway across the region of interest (Fig. 10). This is probably a result of the

Table 5

Absolute permeability values calculated across all pores, and the network of largest pores in the Berea, Bunter and Castlegate samples. As discussed previously the 'largest pores' are those that comprise 60% of the pore volume.

	Permeability [mD]	Permeability of largest pores [mD]
Berea	14	0
Bunter	142	0
Castlegate	495	27

well connected large pores in the Castlegate sample, that allow for a well established, stable pathway for brine to flow across the region of interest (Fig. 10). During subsequent low salinity flooding, brine can flow across the preexisting connected pathway of brine, bypassing oil. As a result, it is not favourable for capillary trapped oil to be mobilised during low salinity flooding in the Castlegate sample [74–78]. In contrast, in the Berea and Bunter samples, there is no connectivity across the region of interests in the brine phase after high salinity waterflooding. Due to a poorly connected network of large pores, brine must invade smaller pores and throats to connect across the samples during high salinity waterflooding. These smaller pores and throats are susceptible to subsequent oil invasion via both distal and local oil snap off events which have been observed in previous experiments to disconnect brine clusters [30,79–81]. As a result, at the start of tertiary low salinity flooding, brine must invade oil-saturated pores and throats to connect across the samples. Therefore, in the Berea and Bunter samples, the tertiary low salinity waterflood behaves somewhat more like a secondary low salinity waterflood as there is no existing brine pathway for low salinity brine to follow and so, it is more favourable for capillary trapped oil to be displaced by invading low salinity brine [74]. This effect, coupled with a wettability alteration (Fig. 6), which can occur when low salinity brine contacts oil saturated pores and oil coated mineral surfaces, likely explains the disparity in oil mobilisation between the three samples. In the Berea and Bunter samples 22% and 20% of the oil in place after high salinity waterflooding is displaced during low salinity flooding, respectively. In the Castlegate sample, this figure is just 11% (Table 4). The connectivity of large pores controls brine distribution during and after secondary high salinity waterflooding, which in turn controls oil mobilisation and production during subsequent tertiary low salinity waterflooding.

This effect of pore topology can also explain the varying degrees of oil mobilisation in different parts of the Bunter sample. The Bunter sample can be split into two discrete sections: the downstream (upper) section, where larger pores are well connected, and the upstream (lower) section, where larger pores are poorly connected. The boundary between these two sections is closely matched by a change in additional recovery after low salinity waterflooding as observed in the saturation profile (Fig. 11). In the downstream section, where large pores are well connected, there is an additional recovery of 1 percentage point after 20 PV of low salinity flooding. In contrast, in the upstream section, there is an additional recovery of 6 percentage points. The three largest brine blobs after both high salinity and low salinity waterflooding are observed in the downstream section of the region of interest. These differences are probably due to the different pore structures observed. In the downstream section, well connected large pores allow for the creation of more stable brine pathways during high salinity flooding
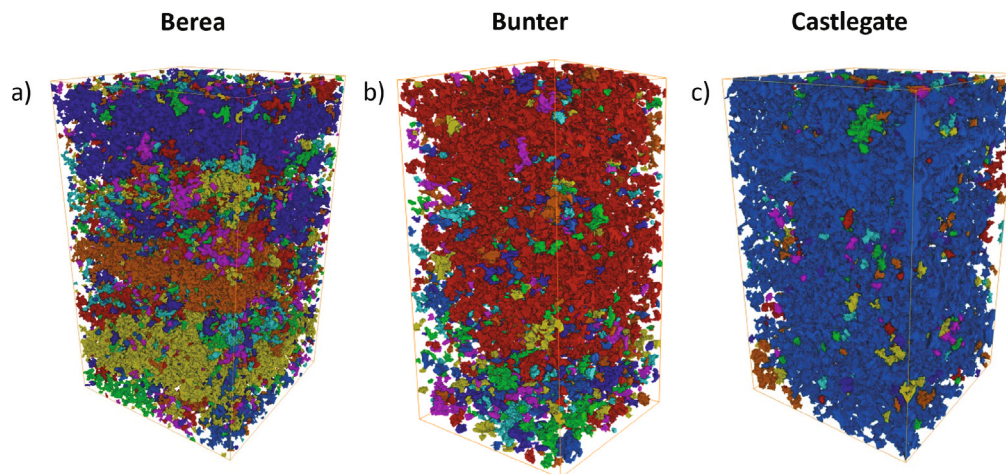
Fig. 9. Volume rendering of largest pores accounting for 60% of pore volume for (a) Berea (b) Bunter (c) Castlegate Each colour represents a separate disconnected region of pores. The Castlegate sample has the most connected large pores with the majority of the pores connected in a single pathway across the region of interest. The Berea and Bunter samples have much poorer connectivity across the largest pores. This is also reflected in the permeability values presented in Table 5. (For interpretation of the references to colour in this figure legend, the reader is referred to the web version of this article.)
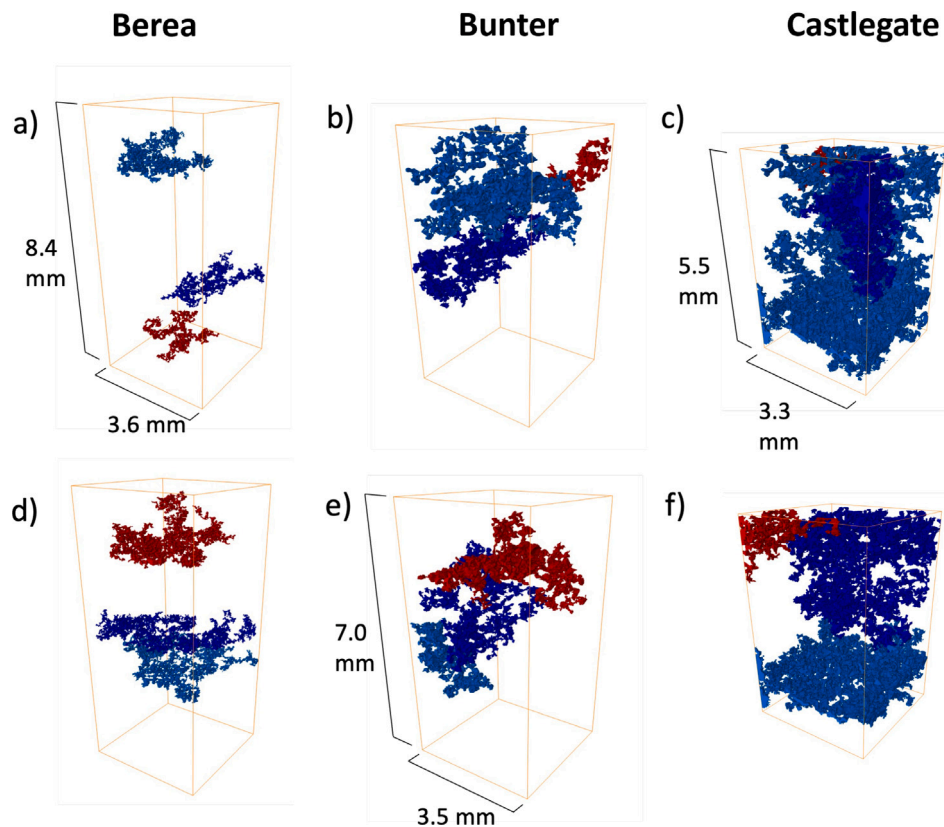

Fig. 10. Volume rendering of the three largest brine blobs after high salinity water flooding for (a) Berea (b) Bunter (c) Castlegate and after 20 PV of low salinity waterflooding for (d) Berea (e) Bunter (e) Castlegate. In the Berea and Bunter samples there is no connected cluster of brine across the region of interest after either HSWF 12PV or LSWF 20PV. In the Castlegate sample there is a connected pathway of brine across the region of interest after HSWF 12PV, this is broken up after LSWF 20PV, but Castlegate still has the largest brine clusters.

and therefore relatively small volumes of oil mobilisation during subsequent low salinity flooding. Conversely, in the upstream section, poorly connected large pores decrease brine connectivity after high salinity flooding and, therefore, increase oil mobilisation during low salinity flooding. Indeed, we observe that the difference in additional oil recovery between the two sections is because of differences in the volume of oil mobilisation during low salinity flooding. There are significantly fewer oil to brine events in the downstream section compared to the
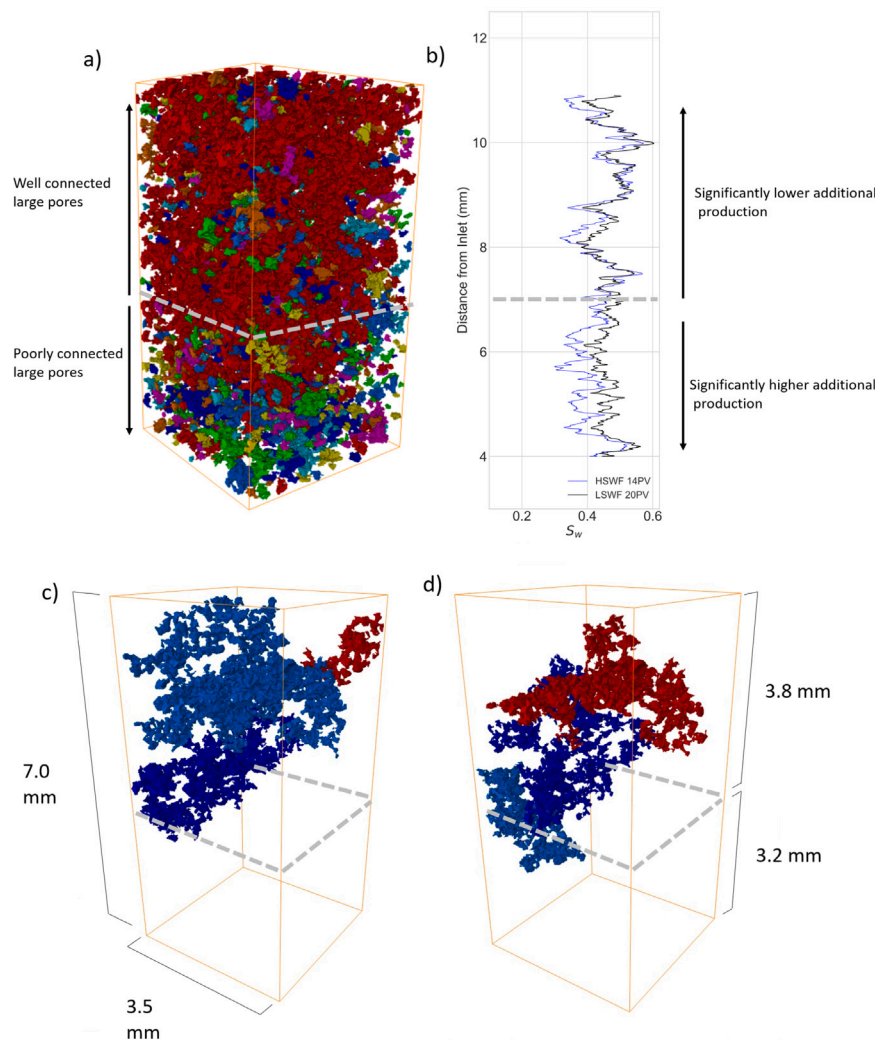
Fig. 11. (a) Volume rendering of the largest pores which make up 60% of the pore space in the Bunter sandstone. Different colours represent disconnected clusters of large pores. (b) Saturation profile for the Bunter sandstone (c) Volume rendering of the largest 3 brine blobs after 12PV of high salinity flooding in the Bunter sandstone and (d) Volume rendering of the largest 3 brine blobs after 20PV of low salinity flooding in the Bunter sandstone. The sample can be broadly be split into two halves (denoted by the grey dotted line). In the downstream (upper) section, the largest pores are well connected, there is lower additional recovery after LSWF 20PV and all three of the largest brine blobs are present. In the upstream (lower) section, there is poor connectivity in the largest pores, there is significantly higher additional recovery after LSWF 20PV. (For interpretation of the references to colour in this figure legend, the reader is referred to the web version of this article.)

upstream section (Fig. 12). Pores which changed from oil occupied to brine occupied during 20 PV of low salinity flooding make up 14% of the total pore volume in upstream section and 10% of total pore volume in downstream section. The evidence from local differences in pore topology and production in the Bunter sample further highlights the impact of pore structure on oil production during low salinity water flooding.

4. Summary and conclusions

In this work, we present the first systematic comparison of pore scale behaviour during low salinity waterflooding in sandstones. We used X-ray micro-CT imaging to observe unsteady state tertiary low salinity waterflooding in Berea, Castlegate, and Bunter sandstone samples all of altered wetting state. Our main findings are as follows:

- Significant additional oil production of 3 and 4 percentage points occurred during low salinity flooding in the Berea and Bunter samples respectively. In contrast, we observe an additional recovery of only 1 percentage point during low salinity waterflooding in the Castlegate sample.

- There was a significant wettability alteration towards more water wet conditions in the Berea and Bunter samples, which responded well to low salinity waterflooding. This wettability alteration led to significant pore occupancy changes in the Berea and Bunter samples, with significant increase in S_w in smaller pores during low salinity waterflooding. There was no systematic wettability alteration observed in the Castlegate sample. We observe a similar yet smaller shift in pore occupancy in the Castlegate sample.

- There were different volumes of oil mobilisation during low salinity flooding in each sample. In the Berea 22% of the oil in place after high salinity flooding was mobilised during low salinity water flooding, this value was 20% and 11% for the Bunter and Castlegate samples respectively. In the Berea, a significant proportion of this mobilised oil was retrapped in the largest pores, so that, the additional recovery was higher in the Bunter sandstone despite having a lower fraction of mobilised oil during low salinity water flooding.

- We hypothesise that pore structure, and in particular the topology of the largest pores, had a significant impact on recovery in each of the samples. In the Castlegate sample, the largest pores are well connected across the sample resulting in a stable, connected
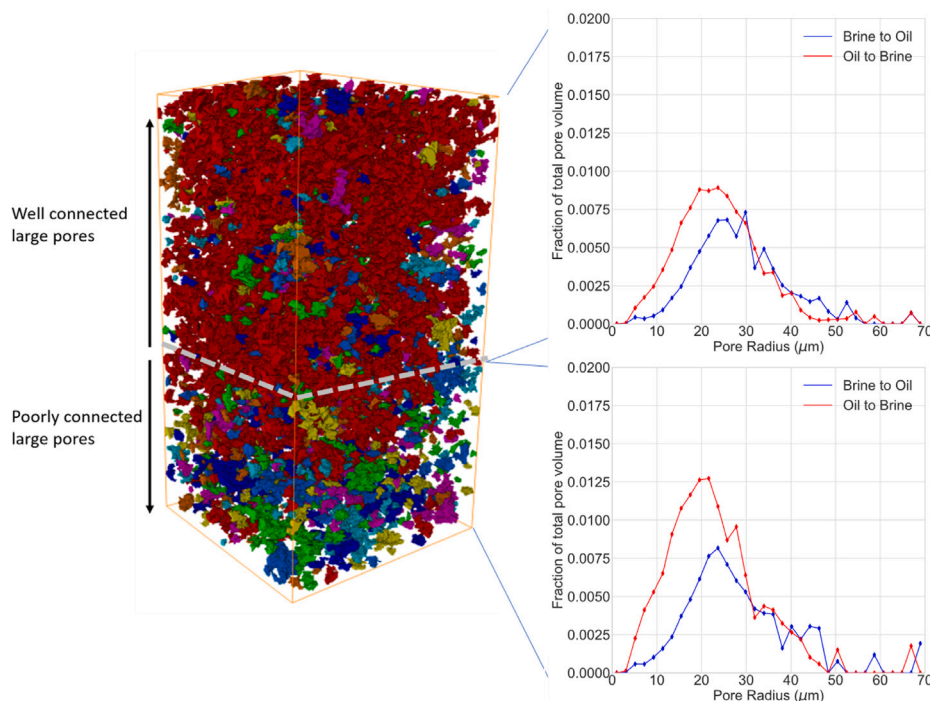
Fig. 12. Volume rendering of largest pores that make up 60% of pore space in Bunter sandstone. The grey dotted lone marks the boundary between two sections—the upper (downstream) section where larger pores are well connected, and the lower (upstream) section where larger pores are poorly connected. For each section the size distribution for all pores (bodies and throats) where saturation changed from oil to brine (red) or brine to oil (blue) between HSWF and LSWF 20PV changes are plotted, is plotted for each section. (For interpretation of the references to colour in this figure legend, the reader is referred to the web version of this article.)

pathway of brine across the largest pores during high salinity waterflooding, which makes oil mobilisation unfavourable during subsequent low salinity flooding. In the Berea and Bunter sandstone, the largest pores are more poorly connected. We hypothesise that in the Berea and Bunter samples, during high salinity water flooding, brine is forced to flow into the small pores and throats during waterflooding, distal and local oil snap off events then break up the brine clusters. During low salinity waterflooding there is no established path for the brine to follow, and so oil mobilisation is more favourable.

Pore structure played an important role in the low salinity response in each sample. Here we have proposed that pore topology can impact the volume of oil mobilisation during tertiary low salinity waterflooding. This, however, does not explain other phenomena, for example, the re-trapping of oil in the largest pores of the Berea sample. There is a complex relationship between pore structure and production. This work acts to highlight this point and offer the first insights into this relationship. Future work should further investigate the relationship between pore structure and recovery, with the ultimate goal of including pore structure in any exhaustive list of necessary conditions for successful low salinity water flooding. Subtle differences in mineralogy and surface characteristics between the three samples could have also impacted the response to low salinity flooding in each case. Future work will also investigate the effect of mineralogy on the pore scale response to low salinity flooding.

CRediT authorship contribution statement

Edward Andrews: Conceptualization, Methodology, Formal analysis, Investigation, Writing – original draft. **Ann Muggeridge:** Conceptualization, Methodology, Writing – review & editing, Supervision. **Alistair Jones:** Conceptualization, Writing – review & editing, Supervision. **Samuel Krevor:** Conceptualization, Methodology, Writing – review & editing, Supervision.

Declaration of competing interest

The authors declare that they have no known competing financial interests or personal relationships that could have appeared to influence the work reported in this paper.

Data availability

Data will be made available on request.

Acknowledgements

References

[1] Morrow NR, Tang G-q, Valat M, Xie X. Prospects of improved oil recovery related to wettability and brine composition. J Pet Sci Eng 1998;20(3–4):267–76.

[2] Tang G-Q, Morrow NR. Influence of brine composition and fines migration on crude oil/brine/rock interactions and oil recovery. J Pet Sci Eng 1999;24(2–4):99–111.

[3] Tang G, Morrow NR, et al. Salinity, temperature, oil composition, and oil recovery by waterflooding. SPE Reserv Eng 1997;12(04):269–76.

[4] Tang G, Morrow NR. Injection of dilute brine and crude oil/brine/rock interactions. In: Washington DC american geophysical union geophysical monograph series, vol.129, 2002, p. 171–9.

[5] Jadhunandan P, Morrow NR, et al. Effect of wettability on waterflood recovery for crude-oil/brine/rock systems. SPE Reserv Eng 1995;10(01):40–6.

[6] Lager A, Webb KJ, Black C, Singleton M, Sorbie KS, et al. Low salinity oil recovery-an experimental investigation. Petrophysics 2008;49(01).

[7] Ligthelm DJ, Gronsveld J, Hofman J, Brussee N, Marcelis F, van der Linde H, et al. Novel waterflooding strategy by manipulation of injection brine composition.. In: EUROPEC/EAGE conference and exhibition. Society of Petroleum Engineers; 2009.

[8] Yousef AA, Al-Saleh SH, Al-Kaabi A, Al-Jawfi MS, et al. Laboratory investigation of the impact of injection-water salinity and ionic content on oil recovery from carbonate reservoirs. SPE Reserv Eval Eng 2011;14(05):578–93.

[9] Yousef AA, Al-Saleh S, Al-Kaabi AU, Al-Jawfi MS, et al. Laboratory investigation of novel oil recovery method for carbonate reservoirs. In: Canadian unconventional resources and international petroleum conference. Society of Petroleum Engineers; 2010.

[10] Rivet S, Lake LW, Pope GA, et al. A coreflood investigation of low-salinity enhanced oil recovery. In: SPE annual technical conference and exhibition. Society of Petroleum Engineers; 2010.

[11] Vledder P, Gonzalez IE, Carrera Fonseca JC, Wells T, Ligthelm DJ, et al. Low salinity water flooding: proof of wettability alteration on a field wide scale. In: SPE improved oil recovery symposium. Society of Petroleum Engineers; 2010.

[12] Lager A, Webb KJ, Collins IR, Richmond DM, et al. Losal enhanced oil recovery: Evidence of enhanced oil recovery at the reservoir scale. In: SPE symposium on improved oil recovery. Society of Petroleum Engineers; 2008.

[13] Shaker Shiran B, Skauge A, et al. Wettability and oil recovery by low salinity injection. In: SPE EOR conference at oil and gas west asia. Society of Petroleum Engineers; 2012.

[14] Cissokho M, Bertin H, Boussour S, Cordier P, Hamon G, et al. Low salinity oil recovery on clayey sandstone: experimental study. Petrophysics 2010;51(05).

[15] Soraya B, Malick C, Philippe C, Bertin HJ, Hamon G, et al. Oil recovery by low-salinity brine injection: Laboratory results on outcrop and reservoir cores. In: SPE annual technical conference and exhibition. Society of Petroleum Engineers; 2009.

[16] Nasralla RA, Nasr-El-Din HA, et al. Double-layer expansion: is it a primary mechanism of improved oil recovery by low-salinity waterflooding? SPE Reserv Eval Eng 2014;17(01):49–59.

[17] RezaeiDoust A, Puntervold T, Austad T, et al. A discussion of the low-salinity EOR potential for a north sea sandstone field. In: SPE annual technical conference and exhibition. Society of Petroleum Engineers; 2010.

[18] Bartels W-B, Mahani H, Berg S, Hassanizadeh S. Literature review of low salinity waterflooding from a length and time scale perspective. Fuel 2019;236:338–53.

[19] Jackson M, Vinogradov J, Hamon G, Chamerois M. Evidence, mechanisms and improved understanding of controlled salinity waterflooding part 1: Sandstones. Fuel 2016;185:772–93.

[20] Berg S, Cense A, Jansen E, Bakker K, et al. Direct experimental evidence of wettability modification by low salinity. Petrophysics 2010;51(05).

[21] Buckley JS, Liu Y, Xie X, Morrow NR, et al. Asphaltenes and crude oil wetting-the effect of oil composition. SPE J 1997;2(02):107–19.

[22] Basu S, Sharma MM. Measurement of critical disjoining pressure for dewetting of solid surfaces. J Colloid Interface Sci 1996;181(2):443–55.

[23] Alotaibi MB, Nasralla RA, Nasr-El-Din HA, et al. Wettability studies using low-salinity water in sandstone reservoirs. SPE Reserv Eval Eng 2011;14(06):713–25.

[24] Sheng J. Critical review of low-salinity waterflooding. J Pet Sci Eng 2014;120:216–24.

[25] Sohrabi M, Mahzari P, Farzaneh SA, Mills JR, Tsolis P, Ireland S, et al. Novel insights into mechanisms of oil recovery by use of low-salinity-water injection. SPE J 2017;22(02):407–16.

[26] Aziz R, Joekar-Niasar V, Martinez-Ferrer P. Pore-scale insights into transport and mixing in steady-state two-phase flow in porous media. Int J Multiph Flow 2018;109:51–62.

[27] Aziz R, Joekar-Niasar V, Martínez-Ferrer PJ, Godinez-Brizuela OE, Theodoropoulos C, Mahani H. Novel insights into pore-scale dynamics of wettability alteration during low salinity waterflooding. Sci Rep 2019;9(1):1–13.

[28] Singh K, Bultreys T, Raeini AQ, Shams M, Blunt MJ. Imbibition in porous media: correlations of displacement events with pore-throat geometry and the identification of a new type of pore snap-off. EarthArXiv; 2019.

[29] Tanino Y, Blunt MJ. Capillary trapping in sandstones and carbonates: Dependence on pore structure. Water Resour Res 2012;48(8).

[30] Blunt MJ. Multiphase flow in permeable media: a pore-scale perspective. Cambridge University Press; 2017.

[31] Holtzman R. Effects of pore-scale disorder on fluid displacement in partially-wettable porous media. Sci Rep 2016;6:36221.

[32] Xu W, Ok JT, Xiao F, Neeves KB, Yin X. Effect of pore geometry and interfacial tension on water-oil displacement efficiency in oil-wet microfluidic porous media analogs. Phys Fluids 2014;26(9):093102.

[33] An S, Yao J, Yang Y, Zhang L, Zhao J, Gao Y. Influence of pore structure parameters on flow characteristics based on a digital rock and the pore network model. J Nat Gas Sci Eng 2016;31:156–63.

[34] Aziz R, Niasar V, Erfani H, Martínez-Ferrer PJ. Impact of pore morphology on two-phase flow dynamics under wettability alteration. Fuel 2020;268:117315.

[35] Namaee-Ghasemi A, Ayatollahi S, Mahani H. Pore-scale simulation of the interplay between wettability, capillary number, and salt dispersion on the efficiency of oil mobilization by low-salinity waterflooding. SPE J 2021;26(06):4000–21.

[36] Bartels W-B, Rücker M, Berg S, Mahani H, Georgiadis A, Fadili A, et al. Fast X-ray micro-CT study of the impact of brine salinity on the pore-scale fluid distribution during waterflooding. Petrophysics 2017;58(01):36–47.

[37] Khishvand M, Alizadeh A, Kohshour IO, Piri M, Prasad R. In situ characterization of wettability alteration and displacement mechanisms governing recovery enhancement due to low-salinity waterflooding. Water Resour Res 2017;53(5):4427–43.

[38] Shabaninejad M, Middlelton J, Fogden A. Systematic pore-scale study of low salinity recovery from berea sandstone analyzed by micro-CT. J Pet Sci Eng 2018;163:283–94.

[39] Andrews E, Muggeridge A, Garfi G, Jones A, Krevor S. Pore-scale X-ray imaging of wetting alteration and oil redistribution during low-salinity flooding of Berea sandstone. Energy & Fuels 2021;35:1197–207.

[40] Sandengen K, Kristoffersen A, Melhuus K, Jøsang LO, et al. Osmosis as mechanism for low-salinity enhanced oil recovery. SPE J 2016;21(04):1–227.

[41] Chen Y, Jha NK, Al-Bayati D, Lebedev M, Sarmadivaleh M, Iglauer S, et al. Geochemical controls on wettability alteration at pore-scale during low salinity water flooding in sandstone using X-ray micro computed tomography. Fuel 2020;271:117675.

[42] Garfi G, John CM, Berg S, Krevor S. The sensitivity of estimates of multiphase fluid and solid properties of porous rocks to image processing. Transp Porous Media 2020;131(3):985–1005.

[43] Khilar KC, Fogler HS, et al. Water sensitivity of sandstones. Soc Petrol Eng J 1983;23(01):55–64.

[44] Shaw JC, Churcher PL, Hawkins BF, et al. The effect of firing on Berea sandstone. SPE Form Eval 1991;6(01):72–8.

[45] Lai P, Krevor S. Pore scale heterogeneity in the mineral distribution and surface area of berea sandstone. Energy Procedia 2014;63:3582–8.

[46] Sen P, Straley C, Kenyon W, Whittingham M. Surface-to-volume ratio, charge density, nuclear magnetic relaxation, and permeability in clay-bearing sandstones. Geophysics 1990;55(1):61–9.

[47] Churcher P, French P, Shaw J, Schramm L, et al. Rock properties of berea sandstone, baker dolomite, and Indiana limestone. In: SPE international symposium on oilfield chemistry. Society of Petroleum Engineers; 1991.

[48] Olivarius M, Weibel R, Hjuler ML, Kristensen L, Mathiesen A, Nielsen LH, et al. Diagenetic effects on porosity–permeability relationships in red beds of the lower triassic bunter sandstone formation in the north German basin. Sediment Geol 2015;321:139–53.

[49] Hjuler ML, Kristensen L. Pre-drilling geothermal assessment of porosity and permeability of the bunter sandstone formation, onshore Denmark. GEUS Bull 2017;38:33–6.

[50] Schmid S, Worden R, Fisher Q. Diagenesis and reservoir quality of the sherwood sandstone (triassic), Corrib field, Slyne basin, west of Ireland. Mar Pet Geol 2004;21(3):299–315.

[51] Pan Z, Trusler JM. Interfacial tensions of systems comprising N2, 7 mass% KI (aq), decane and iododecane at elevated pressures and temperatures. Fluid Phase Equilib 2022;556:113364.

[52] Buades A, Coll B, Morel J-M. A non-local algorithm for image denoising. In: 2005 IEEE computer society conference on computer vision and pattern recognition, Vol. 2. IEEE; 2005, p. 60–5.

[53] Beucher S, Meyer F. The morphological approach to segmentation: the watershed transformation. Math Morphol Image Proc 1993;34:433–81.

[54] Garfi G, John CM, Lin Q, Berg S, Krevor S. Fluid surface coverage showing the controls of rock mineralogy on the wetting state. Geophys Res Lett 2020;47(8):e2019GL086380.

[55] Garfi G, Rücker M, Lin Q, Berg S, John CM, Krevor SC. Pore-by-pore wettability characterization in sandstone and carbonate rocks. In: AGU fall meeting 2020. AGU; 2020.

[56] Bultreys T, Lin Q, Gao Y, Raeini AQ, AlRatrout A, Bijeljic B, et al. Validation of model predictions of pore-scale fluid distributions during two-phase flow. Phys Rev E 2018;97(5):053104.

[57] Raeini AQ, Bijeljic B, Blunt MJ. Generalized network modeling: Network extraction as a coarse-scale discretization of the void space of porous media. Phys Rev E 2017;96:013312.

[58] Dong H, Blunt MJ. Pore-network extraction from micro-computerized-tomography images. Phys Rev E 2009;80(3):036307.

[59] Valvatne PH, Blunt MJ. Predictive pore-scale modeling of two-phase flow in mixed wet media. Water Resour Res 2004;40(7).

[60] Raeini AQ, Bijeljic B, Blunt MJ. Generalized network modeling of capillary-dominated two-phase flow. Phys Rev E 2018;97(2):023308.

[61] Raeini AQ, Yang J, Bondino I, Bultreys T, Blunt MJ, Bijeljic B. Validating the generalized pore network model using micro-CT images of two-phase flow. Transp Porous Media 2019;130(2):405–24.

[62] Lebedeva EV, Fogden A. Micro-CT and wettability analysis of oil recovery from sand packs and the effect of waterflood salinity and kaolinite. Energy & Fuels 2011;25(12):5683–94.

[63] Al-Aulaqi T, Grattoni C, Fisher Q, Musina Z, Al-Hinai S. Effect of temperature, oil asphaltene content, and water salinity on wettability alteration. In: SPE/DGS saudi arabia section technical symposium and exhibition. OnePetro; 2011.

[64] Mohammed I, Mahmoud M, El-Husseiny A, Al Shehri D, Al-Garadi K, Kamal MS, et al. Impact of asphaltene precipitation and deposition on wettability and permeability. ACS Omega 2021;6(31):20091–102.

[65] Yesufu-Rufai S, Rücker M, Berg S, Lowe SF, Marcelis F, Georgiadis A, et al. Assessing the wetting state of minerals in complex sandstone rock in-situ by atomic force microscopy (AFM). Fuel 2020;273:117807.

[66] Nasralla RA, Bataweel MA, Nasr-El-Din HA, et al. Investigation of wettability alteration and oil-recovery improvement by low-salinity water in sandstone rock. J Can Pet Technol 2013;52(02):144–54.

[67] Cense A, Berg S, Bakker K, Jansen E, et al. Direct visualization of designer water flooding in model experiments. In: SPE enhanced oil recovery conference. Society of Petroleum Engineers; 2011.

[68] Mahani H, Berg S, Ilic D, Bartels W-B, Joekar-Niasar V. Kinetics of low-salinity-flooding effect. SPE J 2015;20(01):8–20.

[69] Wei X, Jiang W, Zhang Y, Wang Z, Li X, Wu F. Investigation of clay type on low salinity water flooding using a glass micromodel. Front Energy Res 2020;320.

[70] Rostami P, Mehraban MF, Sharifi M, Dejam M, Ayatollahi S. Effect of water salinity on oil/brine interfacial behaviour during low salinity waterflooding: A mechanistic study. Petroleum 2019;5(4):367–74.

[71] Tetteh JT, Cudjoe SE, Aryana SA, Ghahfarokhi RB. Investigation into fluid-fluid interaction phenomena during low salinity waterflooding using a reservoir-on-a-chip microfluidic model. J Pet Sci Eng 2021;196:108074.

[72] Mohammadi M, Nikbin-Fashkacheh H, Mahani H. Pore network-scale visualization of the effect of brine composition on sweep efficiency and speed of oil recovery from carbonates using a photolithography-based calcite microfluidic model. J Pet Sci Eng 2022;208:109641.

[73] Selem AM, Agenet N, Gao Y, Raeini AQ, Blunt MJ, Bijeljic B. Pore-scale imaging and analysis of low salinity waterflooding in a heterogeneous carbonate rock at reservoir conditions. Sci Rep 2021;11(1):1–14.

[74] Chen Y, Jha NK, Lebedev M, An S, Xie Q, Niasar VJ. Integral effects of initial fluids configuration and wettability alteration on remaining saturation: characterization with X-ray micro-computed tomography. Fuel 2021;306:121717.

[75] Pinerez Torrijos ID, Puntervold T, Strand S, Austad T, Abdullah HI, Olsen K. Experimental study of the response time of the low-salinity enhanced oil recovery effect during secondary and tertiary low-salinity waterflooding. Energy & Fuels 2016;30(6):4733–9.

[76] Zhang Y, Morrow NR. Comparison of secondary and tertiary recovery with change in injection brine composition for crude-oil/sandstone combinations. In: SPE/DOE symposium on improved oil recovery. OnePetro; 2006.

[77] Winoto W, Loahardjo N, Xie XS, Yin P, Morrow NR. Secondary and tertiary recovery of crude oil from outcrop and reservoir rocks by low salinity waterflooding. In: SPE improved oil recovery symposium. OnePetro; 2012.

[78] Gandomkar A, Rahimpour MR. Investigation of low-salinity waterflooding in secondary and tertiary enhanced oil recovery in limestone reservoirs. Energy & Fuels 2015;29(12):7781–92.

[79] Alhosani A, Scanziani A, Lin Q, Foroughi S, Alhammadi AM, Blunt MJ, et al. Dynamics of water injection in an oil-wet reservoir rock at subsurface conditions: invasion patterns and pore-filling events. Phys Rev E 2020;102(2):023110.

[80] Berg S, Ott H, Klapp SA, Schwing A, Neiteler R, Brussee N, et al. Real-time 3D imaging of haines jumps in porous media flow. Proc Natl Acad Sci 2013;110(10):3755–9.

[81] Roof J. Snap-off of oil droplets in water-wet pores. Soc Petrol Eng J 1970;10(01):85–90.